Range Extension Control System for Electric Airplane with Multiple Motors by Optimization of Thrust Distribution Considering Propellers Efficiency

Nobukatsu Konishi and Hiroshi Fujimoto
The University of Tokyo
5-1-5, Kashiwanoha, Kashiwa, Chiba, 227-8561 Japan
Phone: +81-4-7136-3881
Email: konishi@hflab.k.u-tokyo.ac.jp,
fujimoto@k.u-tokyo.ac.jp

Hiroshi Kobayashi and Akira Nishizawa
Institute of Aeronautical Technology
Japan Aerospace Exploration Agency
6-13-1, Osawa, Chofu-shi, Tokyo, 181-0015 Japan
Phone: +81-50-3362-4458
Email: kobayashi.hiroshi2@jaxa.jp,
nishizawa.akira@jaxa.jp

***Abstract*—In the recent years, attention has been gathered in the research field of electric airplanes (EAs), which have electric motors as a power source. EAs have many advantages including low environmental impact and safety. The flight range per charge, however, is shorter than that of conventional airplanes. This paper proposes a range extention control system (RECS) which extends the flight range of EAs by control. It is shown that the power consumption can be minimized by optimizing thrust distribution on multiple propellers with different properties. The effectiveness of the proposed method is verified by simulations and experiments.**

***Keywords*—Electric Airplane, Range Extension Control System, Thrust Distribution, Propeller, Motor Loss**

I. Introduction

A. Background

Considering the increasing demand for air transport, aircrafts are desired to be more energy efficient and safer. Electric airplanes (EAs) can satisfy these demands, because electric motors are used for propulsion. Compared with internal combustion engines (ICEs), motors have the fallowing remarkable advantages [1].

- Response of motor torque is much faster than that of internal combustion engines (over 100 times).
- Distributed installation and independent control are easy.
- Motor torque is measured precisely from motor current.
- Electric motor is more efficient than ICE.

Design of distributed electric propulsion aircraft [2] and study of decrease in ground–run distance [3] were conducted by utilizing the above above advantages. And also EA with fault tolerance was developing from battery to configure [4] [5].

EAs, however, have shorter mileage per charge than the conventional airplanes [6]. For example, the flying range of EAs, which is officially announced, is less than half that of ICE airplane [7], therefore it is necessary to solve this problem.

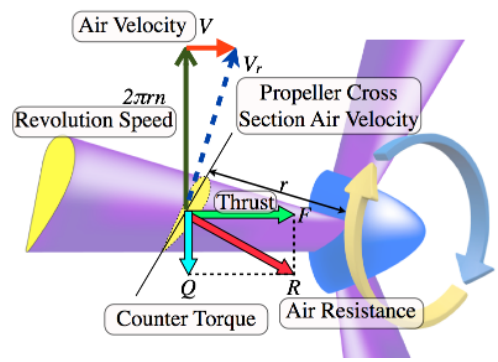

Fig. 1: Principle of propeller cross section[11].

B. Objective

The purpose of this study is to extend the range of EAs by control. The authors' research group proposed range extension control systems (RECSs) for electric vehicles [8] [9]. Although RECS for EA to optimize the propeller pitch angle was proposed in [10], this application of the RECS was only for single propeller airplane.

In order to further extend the flying range, the airplane studied in this paper is assumed to have multiple propellers and motors like the assumption in [2]. Multiple electric propulsions can be optimized for the low speed aerodynamic, propulsive, and acoustic requirements without the complexity of variable pitch. Specifically, a model-based RECS during straight flying is proposed by using multiple propellers which have different characteristics by each. This method considers airspeed, acceleration, and drives thrust distribution ratio that can minimize input power to obtain high efficiency.

II. Modeling

In this chapter, the models of propeller dynamics and power consumption are explained.

A. Propeller Dynamics

Fig. 1 shows the cross section of a propeller blade at distance r from hub [11]. While flying, the propeller cross

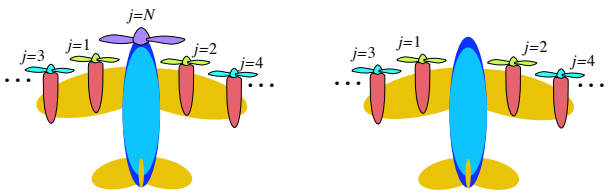

(a) $N = 2i + 1$ (b) $N = 2i$

Fig. 2: Propeller position.

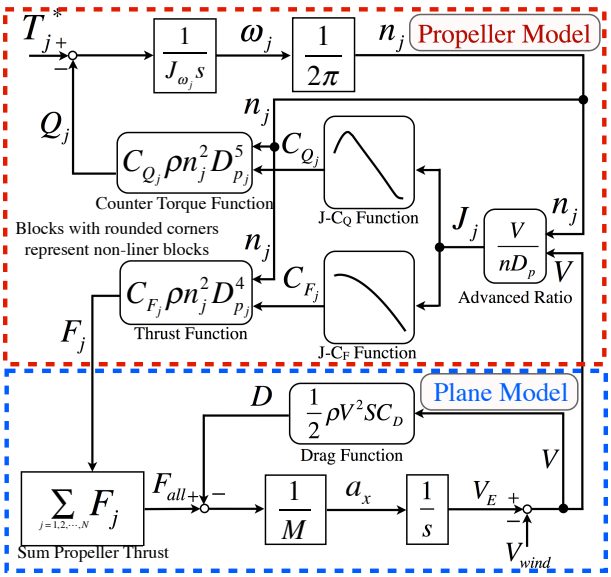

Fig. 3: Model block of plane with multiple propellers.

section moves as a composition of rotation and forward motion. Therefore, the cross section moves as a spiral. Assume the airflow is parallel to the axis of propeller. Airspeed is the relative velocity between the air and airplane. Counter torque $\mathbf{R}$ is generated by the blade of propeller, and $\mathbf{R}$ can be resolved into the direction of the motion of the airplane "thrust" $\mathbf{F}$ and the direction of propeller revolution "counter torque" $\mathbf{Q}$. Assume the air density is ρ, the propeller whose diameter D_p rotates at the propeller revolution speed n, and generates the thrust $F = \mathbf{F}$ and the counter torque $Q = |\mathbf{Q}|$ which can be express as

$$F = C_F(J)\rho n^2 {D_p}^4, \quad (1)$$
$$Q = C_Q(J)\rho n^2 {D_p}^5, \quad (2)$$

where C_F is propeller thrust coefficient, and C_Q is propeller counter-torque coefficient. Generally, each of them is a function of advance ratio J which is defined as

$$J = \frac{V}{nD_p}, \quad (3)$$

where V is the airspeed.

B. Motion Equation of Plane

When the airplane with N propellers moves straight at airspeed V and accelerates at a_x, the equations of plane dynamics is expressed as

$$Ma_x = F_{\text{all}} - D(V), \quad (4)$$

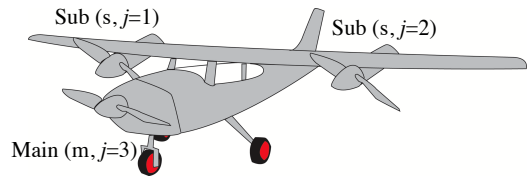

Fig. 4: Plane with 3 propellers.

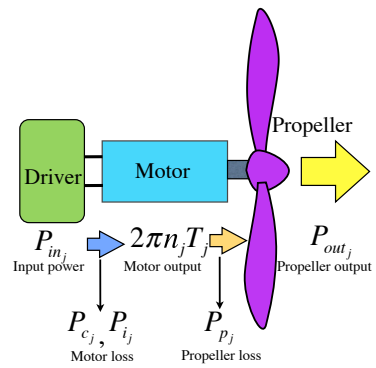

Fig. 5: Diagram of propeller power consumption.

where M is airplane mass, F_{all} is total thrust, and $D(V)$ is air drag. $D(V)$ is expressed as

$$D(V) = \frac{1}{2}C_D\rho V^2 S, \quad (5)$$

where C_D is air drag coefficient, and S is wing area. A propeller thrust F_j after distribution is defined as Eq. (6). The subscript j represents a propeller position, in other words $j \in \{1, 2, \cdots, N\}$. Fig.2 shows the propeller position.

$$F_j(k) = k_j F_{\text{all}}, \quad (6)$$
$$\sum_{j=1,2,\cdots} k_j = 1. \quad (7)$$

Distribution ratio k should always satisfy with Eq. (7). Moreover it is necessary to assume Eq. (8) in order not to generate yaw moment at a straight advancing motion,

$$F_i = F_{i+1} \quad (i = 1, 3, 5, \cdots, N-1). \quad (8)$$

The model of airplane with multiple propellers can be expressed as Fig. 3, provided that wind velocity V_{wind} is ignored, and airspeed V is equal to groundspeed V_E.

Fig. 4 illustrates an airplane with one propeller at the nose and two at left and right wings respectively. The nose position is regarded as "main," and the others are regarded as "sub" in this paper. The relationship between k and F_j is represented below at this situation.

$$F_m(k) = kF_{\text{all}} \quad (j = 3), \quad (9)$$
$$F_s(k) = \frac{1-k}{2}F_{\text{all}} \quad (j = 1, 2). \quad (10)$$

From Eqs. (1), (3), (6), Eq. (11) is obtained as

$$F_j(k) = C_{F_j}\left(\frac{V}{n_j D_{p_j}}\right)\rho {n_j}^2 {D_{p_j}}^4. \quad (11)$$

TABLE I: Relationship of distribution ratio and thrust.

k	Main	Sub×2
0	0	F_{all}
0.33	$\frac{1}{3}F_{\mathrm{all}}$	$\frac{2}{3}F_{\mathrm{all}}$
1	F_{all}	0
k_{opt}	$k_{\mathrm{opt}}F_{\mathrm{all}}$	$(1-k_{\mathrm{opt}})F_{\mathrm{all}}$

TABLE II: Propeller characteristics.

positon name	Main	Sub
propeller diameter D_p	229 mm	203 mm
propeller pitch	96.5 mm	203 mm
propeller inertia J_ω	2.25×10^{-5} kg·m^2	1.58×10^{-5} kg·m^2

Therefore, n_j is a function of k, and Q_j is also a function of k from Eq. (2). As the inertia of the propeller is smaller enough than counter torque, an assumption is made as

$$T_j(k) = Q_j(k). \tag{12}$$

Next, propeller efficiency η_{p_j} is represented below from Eqs. (1)–(3) and (12).

$$\eta_p = \frac{FV}{2\pi nT} = \frac{C_F(J)\rho n^2 {D_p}^4 V}{2\pi C_Q(J)\rho n^3 {D_p}^5} = \frac{J}{2\pi}\frac{C_F(J)}{C_Q(J)}. \tag{13}$$

C. Modeling of Power Consumption

The model of the power consumption is created, considering propeller efficiency and motor loss. Fig. 5 illustrates the power consumption conception of the single propeller and motor. If the motor mechanical loss is ignored, power consumption P_{in_j} is represent as

$$P_{in_j} = P_{out_j} + P_{p_j} + P_{c_j} + P_{i_j}, \tag{14}$$

where P_{out_j} is the propeller mechanical output, P_{p_j} is the propeller loss, P_{c_j} is the motor copper loss, and P_{i_j} is the motor iron loss.

$$P_{out_j}(k) = F_j(k)V \tag{15}$$

From Eq. (13), P_{p_j} is expressed as

$$P_{p_j}(k) = \frac{1-\eta_{p_j}(k)}{\eta_{p_j}(k)}P_{out_j}(k). \tag{16}$$

Next, the relationship between P_{out_j} and motor mechanical output $2\pi n_j(k)T_j(k)$ is established by Eq.(17).

$$P_{out_j}(k) = 2\pi n_j(k)T_j(k) - P_{p_j}(k). \tag{17}$$

Motor copper loss P_{c_j} is expressed by motor winding resistance R_{e_j} and motor torque constant K_{t_j} as

$$P_{c_j}(k) = R_{e_j}\left(\frac{T_j(k)}{K_{t_j}}\right)^2. \tag{18}$$

In this paper, equivalent circuit model [12] is used to represent iron loss. Motor iron loss P_{i_j} can be expressed as

$$P_{i_j}(k) = \frac{{\omega_{e_j}(k)}^2}{R_{i_j}}\left\{\left(\frac{L_j}{K_{t_i}}\right)^2 {T_j(k)}^2 + {K_{e_j}}^2\right\}, \tag{19}$$

where R_{i_j} is the equivalent iron loss resistance of each motor, L_{d_j} is inductance, ω_{e_j} is the electrical angular velocity which is defined as Eq. (20), and K_{e_j} is the induced voltage constant which is defined as Eq. (21).

$$\omega_{e_j}(k) = 2\pi n_j(k)p_{n_j}, \tag{20}$$

$$K_{e_j} = \frac{K_{t_j}}{p_{n_j}}. \tag{21}$$

From Eqs.(14)–(21), P_{in_j} is obtained as

$$P_{in_j}(k) = 2\pi n_j(k)T_j(k) + \frac{R_{e_j}{T_j(k)}^2}{{K_{t_j}}^2} + P_{i_j}(k). \tag{22}$$

From above equations, Total power consumption $P_{in_{\mathrm{all}}}$ is expressed as

$$P_{in_{\mathrm{all}}}(k) = \sum_{j=1,2,3,\cdots} P_{in_j}(k). \tag{23}$$

Since $P_{in_{\mathrm{all}}}(k)$ is a function of k, optimal distribution ratio k_{opt} satisfies $\partial P_{in_{\mathrm{all}}}/\partial k|_{k=k_{\mathrm{opt}}} = 0$. It, however, is difficult to solve this equation analytically. In this paper, k_{opt} is calculated by the golden section search to minimize the power consumption, by making the k_{opt} map with regard to V and a_x.

III. Simulation

In this chapter, the effectiveness of the proposal method is conformed by two kinds of simulation, supposing the plane is equipped with 3 propellers.

A. Conditions

The airplane parameter are decided by scaling a real airplane by referring to [6]. Distribution ratio k varies between 0 and 1, where $k = 0$ means that the total thrust is generated by only two sub propellers, and $k = 1$ means that the total thrust is generated by only main propeller. Table I shows the relationship between distribution ratio and thrust. In addition, there is no change of air drag coefficient C_D in this section.

Main and sub propellers have different parameters as given in Table II. These characteristics, J–C_F and J–C_Q are measured by wind tunnel, and are shown in Fig. 6(a) and (b) respectively. For the main propeller, thrust coefficient C_F and counter-torque coefficient C_Q are small. On the other hand, both coefficients for the sub propeller are large. Fig. 6(c) and (d) shows each propeller efficiency η_p. From this viewpoint,

TABLE III: Motor characteristics.

motor winding resistance R_e	0.299 Ω
core loss resistance R_i	2.38 Ω
inductance L	0.0823 mH
torque constant K_t	30.2 mNm/A
number of pole pairs p_n	1

TABLE IV: Plane characteristics [13].

length	1.42 m
width	1.78 m
wing area S	0.440 m^2
gross weight M	4.42 kg
lift coefficient C_L	0.580
drag coefficient C_D	0.048

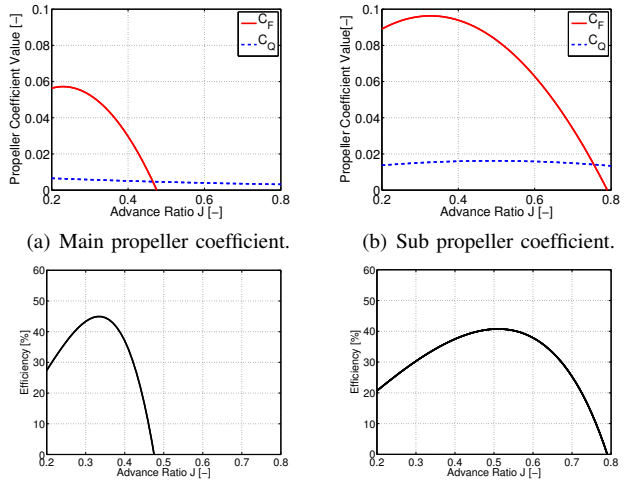

(a) Main propeller coefficient. (b) Sub propeller coefficient.

(c) Main propeller efficiency. (d) Sub propeller efficiency.

Fig. 6: Propeller characteristics.

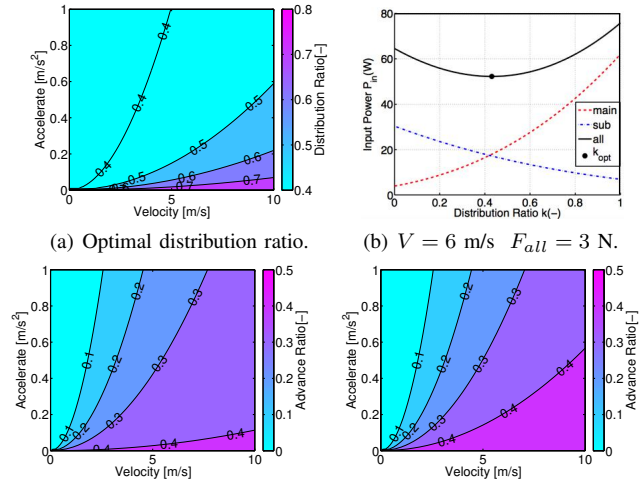

(a) Optimal distribution ratio. (b) $V = 6$ m/s $F_{all} = 3$ N.

(c) Main advance ratio. (d) Sub advance ratio.

Fig. 7: Simulation results.

while main propeller have a good efficiency at low advance ratio range, sub propeller is good at high advance ratio range.

B. Optimal Distribution Ratio Calculation

In this section, calculation of optimal thrust distribution is conducted based on the values of Table III and Table IV referring to [13].

Fig. 7 shows simulation results. Fig. 7(a) illustrates the calculation result of the k_{opt} map. k_{opt} increases with the increase of airspeed and decreases with the increase of acceleration. The range of k_{opt} is from 0.4 to 0.8, so it tends to use sub propellers more.

Fig. 7(b) shows the relationship between distribution ratio k and the consumption power P_{in} at $V = 6$ m/s and $F_{\mathrm{all}} = 3$ N. From Eq. (4), acceleration is equivalent to $a_x = 0.57$ m/s^2 at this condition. The black point indicates k_{opt} position which is obtained from the k_{opt} map. The consumption power is calculated considering the propeller inertias. k_{opt} from the model corresponds to the ratio of the minimum of $P_{in_{\mathrm{all}}}$.

Fig. 7(c) and (d) illustrate advance ratio J of main and sub propellers when $k = k_{\mathrm{opt}}$. Refer to Fig. 6(a), main propeller is positively used around the highest efficiency area, because the efficiency of main propeller is higher than that of sub one. On the other side, J mainly depends on the thrust because sub propeller has good efficiency over wide J range. In addition, it is necessary to obtain big thrust by increase the revolution speed on large accelerate area, so J decreases consequently at both of propellers.

C. Evaluation by Airspeed Pattern

In this section, to demonstrate the effectiveness of the proposal method, evaluation of airspeed pattern is conducted. Fig. 8(a) shows the airspeed pattern, which is composed of two cruising phases, 3.0 m/s and 8.0 m/s, and one accelerating phase, 0.5 m/s^2. In this simulation, the thrust is assumed to output with no delay from the reference by the feedforward based on Eq. (1).

The results of the simulation show at Fig. 8(b)–(h). As Fig. 8(b), there are 4 kinds of the distribution ratio in this simulation, $k = 0, 0.33, 1,$ and k_{opt}. k_{opt} is obtained from the k_{opt} map which is calculated from airspeed reference and accelerating. Next, as Fig. 8(c) and (d), total thrust F_{all} is distributed to main and sub propellers . Fig. 8(e) and (f) illustrates advance ratio J transition of main and sub one.

Fig. 8(g) shows the consumption energy of the cruising phase ($0 \leq t \leq 5, 15 \leq t \leq 25$) and the accelerate phase ($0 \leq t \leq 5$). When $k = k_{\mathrm{opt}}$, the consumption energy is reduced by 5% compared to $k = 0.33$. These results demonstrates effectiveness of the proposal method.

In addition, total efficiency η_{all} is defined as

$$\eta_{\mathrm{all}} = \frac{\sum P_{out_j}}{\sum P_{in_j}}. \tag{24}$$

The efficiency transition of airspeed pattern shows in Fig. 8(h). Maximum efficiency is obtained by the optimal distribution ratio.

IV. Experiment

In this chapter, the effectiveness of the proposal method is conformed by experiments, supposing the plane with 3 propellers are at the same condition as the simulation.

A. Experimental Setup

In this part, the experimental setup shown in Fig. 9 made for this research will be explained. The unit consists of liner guide, force sensor, motor mount, motor, encoder, propeller, anemometer, and wind tunnel. The propeller is connected to the motor, and the thrust which the propeller generates is measured by an force sensor. The propeller is set at 50 mm from the opening of the wind tunnel, so that the axis of the propeller is parallel with the wind.

It is impossible to make an experiment with 3 propellers because the limited of the wind tunnel. This is the reason that the total power consumption is the summation of three propellers' power consumption which are measured individually.

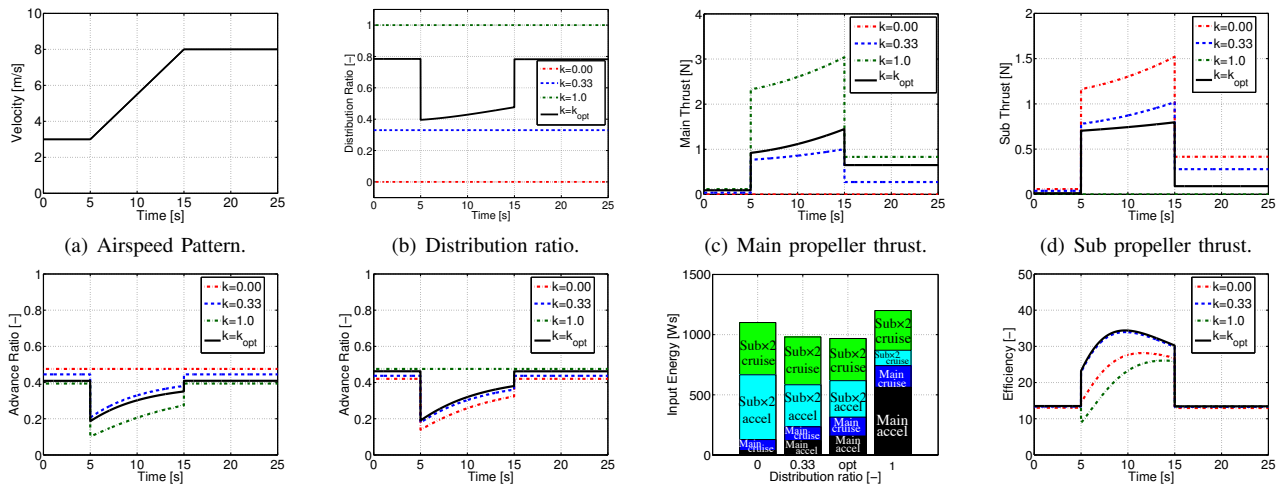

(a) Airspeed Pattern. (b) Distribution ratio. (c) Main propeller thrust. (d) Sub propeller thrust.

(e) Main avance ratio. (f) Sub advance ratio. (g) Total energy. (h) Efficiency.

Fig. 8: Simulation results of airspeed pattern moving.

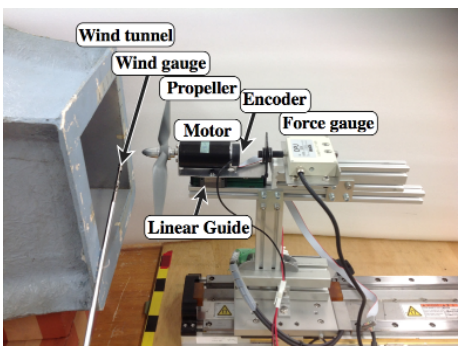

Fig. 9: Picture of experimental equipment.

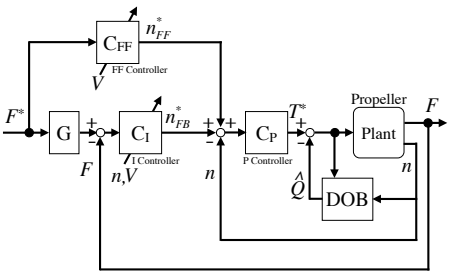

Fig. 10: Thrust control system [14].

The power consumption is the product of the input current and the input voltage at the motor driver. Acceleration a_x is calculated from Eqs. (4) and (5), and all the parameters of the experiment are the same as that of the simulation.

It is necessary to control thrust of propeller, because there is disturbance and modeling error in the experiment. Fig. 10 shows the thrust control system, refer to [14]. This system is composed of a feedforward loop and two feedback loops (the revolution speed and the thrust). The input is thrust reference F_j^* and these controllers generate the motor torque reference T_j^*. A disturbance observer is employed in compensate the counter torque Q for T_j^*.

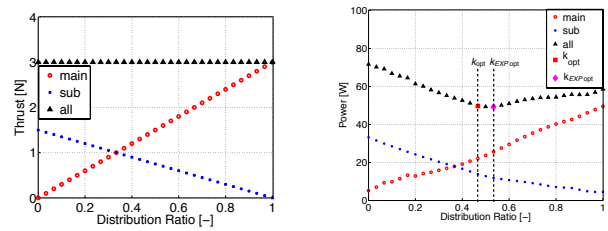

(a) Thrust distribution. (b) Input power.

Fig. 11: Optimal distribution experiment results.

B. Optimal Distribution Ratio Experiment

In this section, a basic experiment to conform optimal distribution ratio is explained. Fig. 11 are the results of the experiment. Fig. 11(a) illustrates the relationship between k and F_j which is distributed at $V = 6$ m/s and $F_{\mathrm{all}} = 3$ m/s. Fig. 11(b) shows the transition of the power consumption, main, sub, and total. From the experimental results, the experimental distribution ratio of the minimum power consumption $k_{\mathrm{EXP_{opt}}}$ is 0.52. From the k_{opt} map, the optimal distribution ratio k_{opt} is 0.43 which is approximately equal to the experimental one. The power consumption is optimized by k_{opt} which is calculated from the model. It is succeed that the power consumption when $k = k_{\mathrm{opt}}$ reduce by 8 % as compared with when the equal distribution $k = 0.33$. These results show that the power consumption is reduced, and demonstrate the effectiveness of the proposal method.

C. Experiment of the Velocity Pattern

Airspeed is controlled by the wind tunnel to make an airspeed pattern. Thrust of propeller is controlled depending on airspeed.

Fig. 12 shows the experimatal results. Since Fig. 12(a) and Fig. 12(b) are same as the simulation. Airspeed pattern starts from 3 m/s, accelerates at 0.5 m/s^2 for five seconds, and cruises

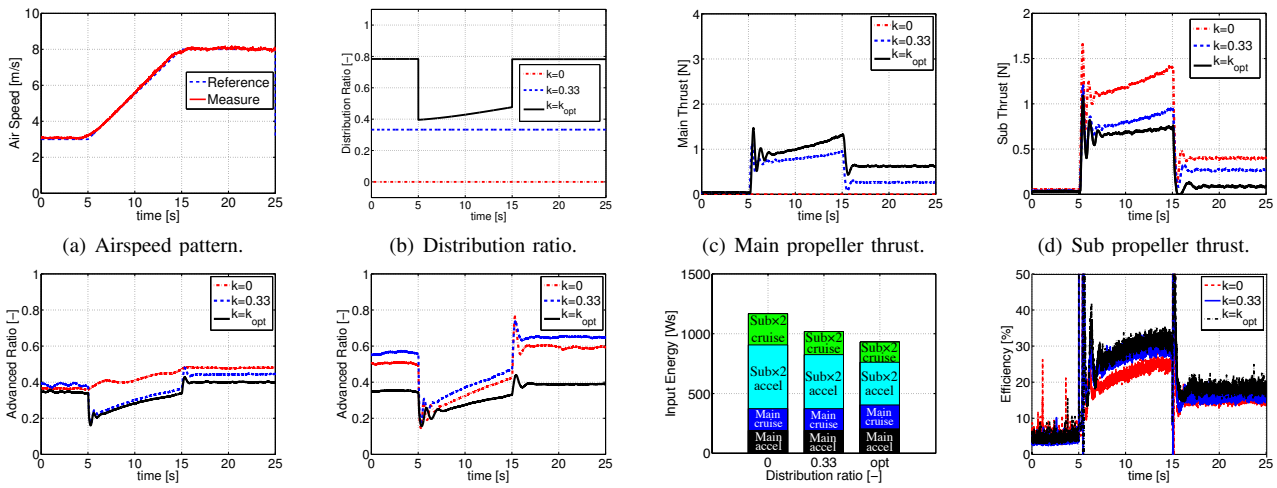

(a) Airspeed pattern. (b) Distribution ratio. (c) Main propeller thrust. (d) Sub propeller thrust.

(e) Main advance ratio. (f) Sub advance ratio. (g) Total energy. (h) Efficiency.

Fig. 12: Experimental results of airspeed pattern moving.

at 8 m/s. Distribution ratio is $k = 0, 0.33, k_{\mathrm{opt}}$. $k = 1$ is not measured, because the maximum limitation of the motor torque is too small to make thrust F_{all} by only the main propeller.

From Fig. 12(c) and Fig. 12(d), the main and sub propeller thrust F_{m}, F_{s} are vibratory. This is due to the influences of sensor noise and resolution of motor encoders. Fig. 12(e) and Fig. 12(f) shows main and sub advance ratio J_{m}, J_{s}. Each propeller takes advance ratio which makes high efficiency depending on the airspeed.

Fig. 12(g) shows the energy consumption during accelerating, cruising and overall airspeed pattern. The case of k_{opt} achieves reduction of energy consumption compared with the case of when $k = 0, 0.33$. Since the experimental results include mechanical loss and driver loss, energy consumption of experiment is different from that of simulation.

In addition, Fig. 12(h) illustrates the transition of total efficiency η_{all}. The optimal distribution makes the highest efficiency during overall airspeed pattern in experiment.

V. Conclution

This paper aimed at extending flying range of EAs through optimizing thrust distribution. That is, the power consumption of EAs can be minimized by using the proposed approach. The effectiveness of the proposed model–based method was verified by simulations and the experiments.

For future works, the effectiveness of the proposal method on other airspeed patterns was verified in front of the large wind tunnel and the energy consumption will be measured simultaneously. Furthermore, it is necessary to consider the mass of the propellers and motors depending on the number of them, and to compare with variable pitch propeller system.

References

[1] Y. Hori, "Future vehicle driven by electricity and control–research on four–wheel–motored UOT Electric March Ⅱ," IEEE Trans. on Ind. Electron, Vol. 51, No. 5, pp. 954–962 (2004).

[2] A. M. Stall, J. B. Bevirt, M. D. Moore, J. Fredericks, and N. K. Borer, "Drag Reduction Through Distributed Electric Propulsion," Aviation Technology. Integration and Operations Conference, pp. 16–20 (2014).

[3] H. Kobayashi, A. Nishizawa, "Decrease in Ground–Run Distance of Airplanes by applying Electrically Driven Wheels," the 27th International Congress of the Aeronautical Sciences, pp. 1–8 (2010).

[4] P. Guglielmi, G. Pellegrino, G. Griva, F. Villata, P. Maggiore, M. Bruno, R. Lamberti, and F. Gadrino, "A Direct-Drive Solution for Hydrogen Supplied All-Electric Airplane," the 35th Annual Conference of the IEEE Industrial Electronics Society, pp. 2525–2530, (2009).

[5] I. Pazdera, P. Prochazka, D. Cervinka, and B. Klima, "Electric Drivetrain of the Small Airplane and Mutual Interaction of this Drivetrain," the 40th Annual Conference of the IEEE Industrial Electronics Society, pp. 4622–4627, (2013).

[6] M. D. Moore and Bill Fredericks, "Misconceptions of Electric Propulsion Aircraft and their Emergent Aviation Markets," the 52nd Aerospace Sciences Meeting AIAA SciTech, 17p (2014).

[7] J. Langelaan (Green Flight Challenge), "Aircraft Design and Flight Planning for Extreme Fuel Efficiency," Journal of Aircraft, Vol. 50, No. 3, pp. 832–846 (2013).

[8] S. Harada and H. Fujimoto, "Range Extension Control System for Electric Vehicle during Acceleration and Deceleration Based on Front and Rear Driving–Braking Force Distribution Considering Slip Ratio and Motor Loss," the 39th Annual Conference of the IEEE Industrial Electronics Society, pp.6624–6629 (2013).

[9] W. Yafei, F. Hiroshi, H. Shinji, "Range Extension Control System for Electric Vehicles by LTI Modeling with Generalized Frequency Variable," American Control Conference, pp. 3838–3843, (2014).

[10] N. Kobayashi, H. Fujimoto, Y. Hori, H. Kobayashi, and A. Nishizawa, "A study of Range Extension Control System by Optimization of Motor Torque and Propeller Pitch Angle for Electric Airplane," IEE of Japan Technical Meeting Record, IIC–13–095, MEC–13–095, pp. 31–36 (2013) (in Japanese).

[11] Karl. H, "Aircraft Propeller Handbook", The Ronald Press Company, New York (1937).

[12] S. Morimoto, Y. Tong, Y. Takeda, and T. Hirasa, "Loss Minimization Control of Permanent Magnet Synchronous Motor Drives," IEEE trans. on Ind. Electron, Vol. 41, No. 5, pp. 511–517 (1994).

[13] D. L. Kohlman, "Flight Test Results for an Advanced Technology light Airplane," Journal of Aircraft. Vol. 16, No. 4, pp. 250–255 (1979).

[14] K. Takahashi, H. Fujimoto, Y. Hori, H. Kobayashi, and A. Nishizawa, "Modeling of Propeller Electric Airplane and Thrust Control using Advantage of Electric Motor," The 13th International Workshop on Advanced Motion Control. pp. 699–704 (2014).